Electronic Supplementary Material (ESI) for Catalysis Science & Technology.

Supplementary Information

Probing the Nanoscale Driving Forces for Adsorbate-Induced $Rh_{50}Pd_{50}$ Nanoparticle Reconstruction via Mean-Field Models of Multi-Faceted Nanoparticles

Shuqiao Wang[1] and Alyssa J.R. Hensley[1]*

[1] Department of Chemical Engineering and Materials Science, Stevens Institute of Technology, Hoboken, NJ 07030
* Corresponding Author: ahensley@stevens.edu

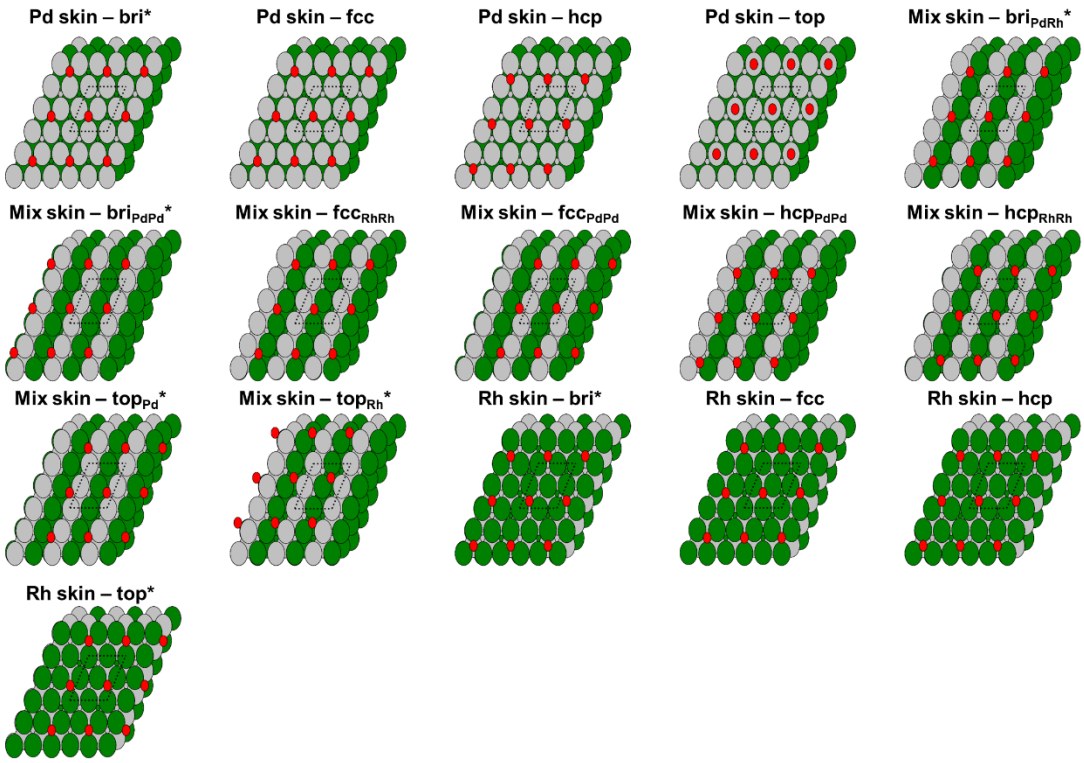

Figure S1. Top views of sites tested for 0.25 ML O* adsorption on $Rh_{50}Pd_{50}$(111). The silver, green, and red spheres represent Pd, Rh, and O, respectively. The sites marked with a * indicate site shifting upon optimization. See Table S1 for adsorption energies.

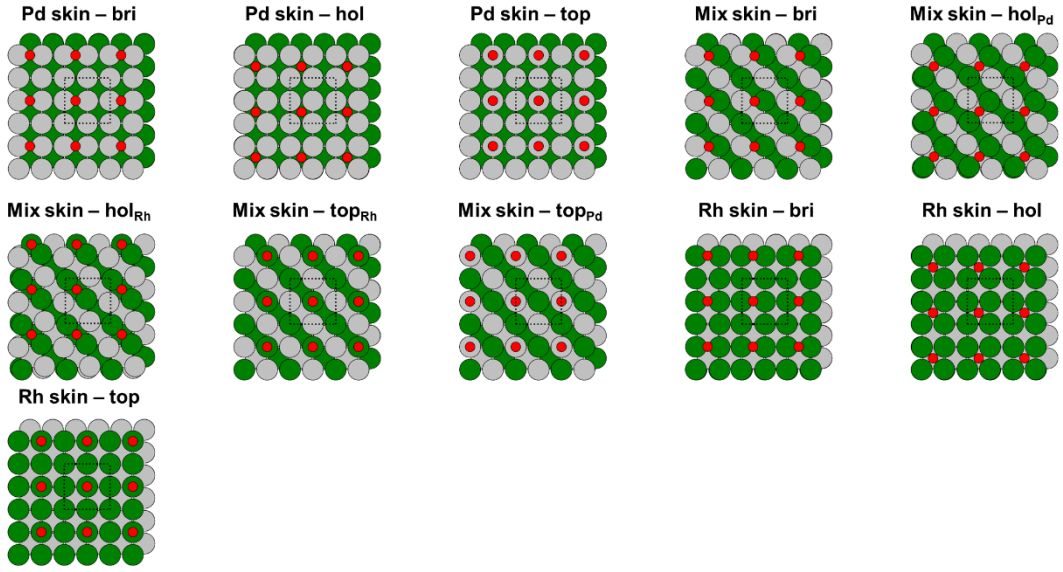

Figure S2. Top views of sites tested for 0.25 ML O* adsorption on $Rh_{50}Pd_{50}$(100). The silver, green, and red spheres represent Pd, Rh, and O, respectively. See Table S2 for adsorption energies.

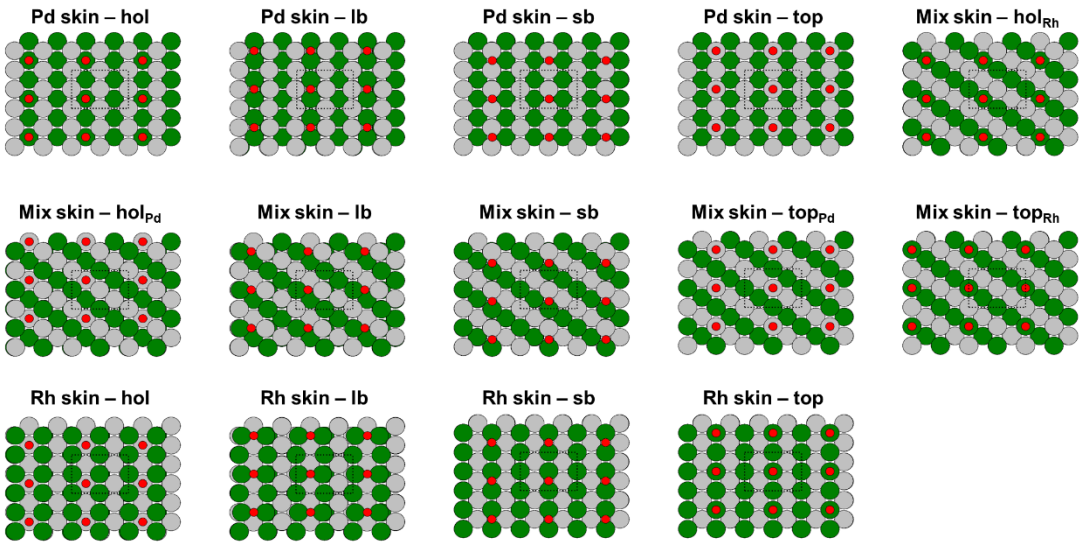

Figure S3. Top views of sites tested for 0.25 ML O* adsorption on $Rh_{50}Pd_{50}$(110). The silver, green, and red spheres represent Pd, Rh, and O, respectively. See Table S3 for adsorption energies.

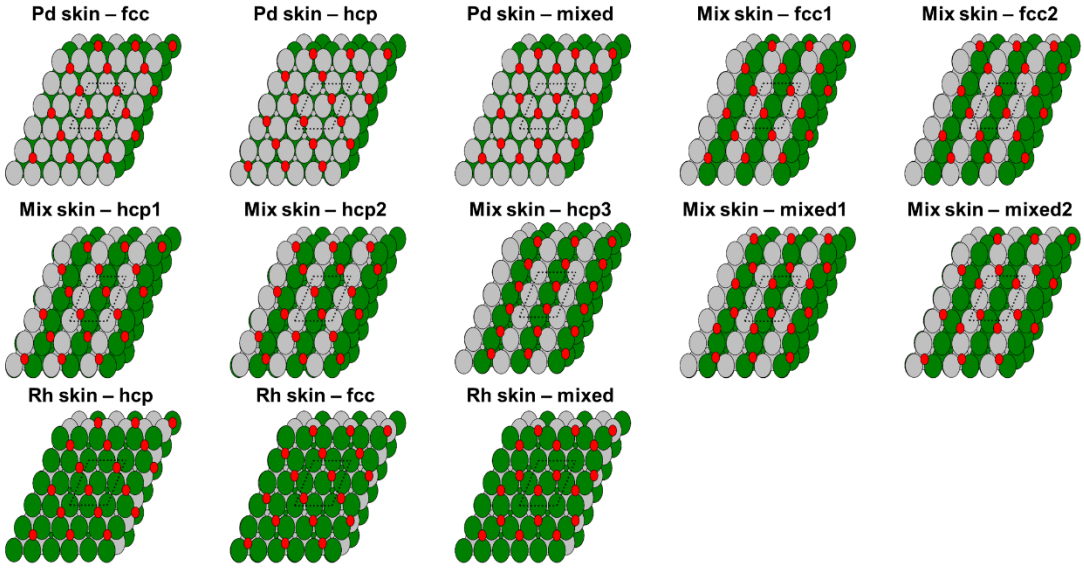

Figure S4. Top views of sites tested for 0.50 ML O* adsorption on $Rh_{50}Pd_{50}$(111). The silver, green, and red spheres represent Pd, Rh, and O, respectively. See Table S1 for adsorption energies.

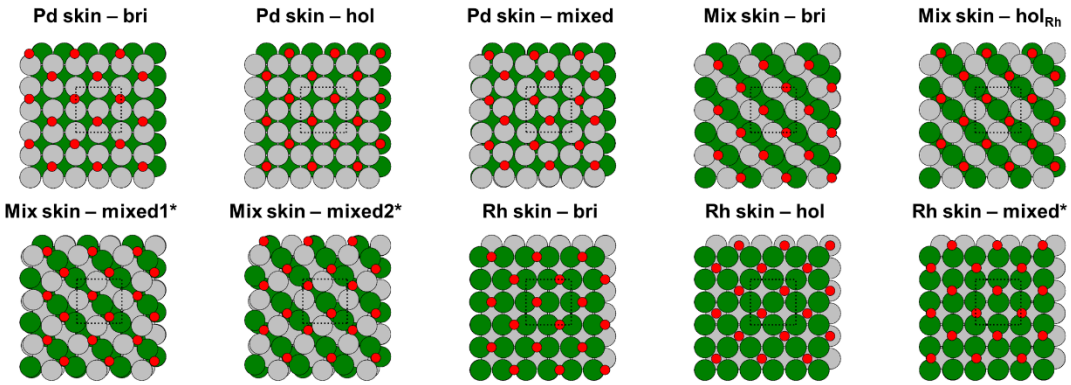

Figure S5. Top views of sites tested for 0.50 ML O* adsorption on $Rh_{50}Pd_{50}$(100). The silver, green, and red spheres represent Pd, Rh, and O, respectively. The sites marked with a * indicate site shifting upon optimization. See Table S2 for adsorption energies.

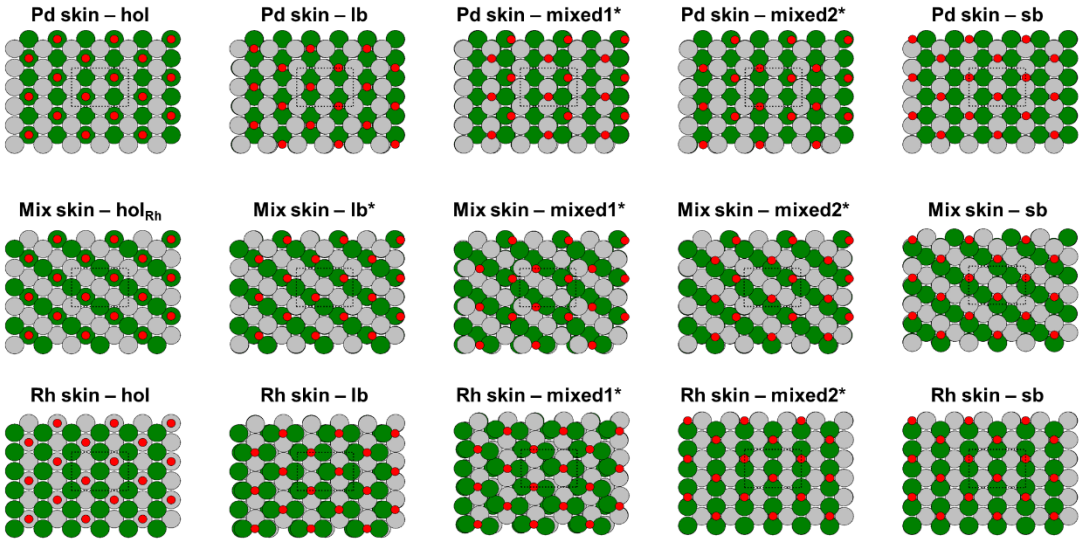

Figure S6. Top views of sites tested for 0.50 ML O* adsorption on $Rh_{50}Pd_{50}$(110). The silver, green, and red spheres represent Pd, Rh, and O, respectively. The sites marked with a * indicate site shifting upon optimization. See Table S3 for adsorption energies.

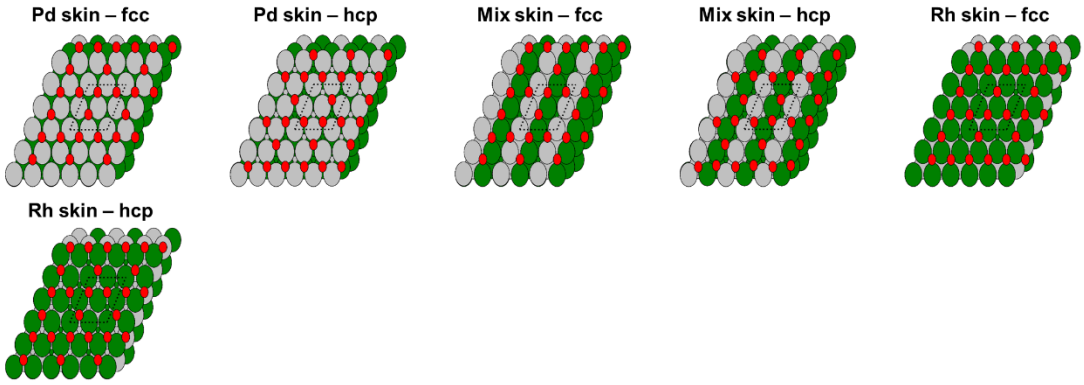

Figure S7. Top views of sites tested for 0.75 ML O* adsorption on $Rh_{50}Pd_{50}$(111). The silver, green, and red spheres represent Pd, Rh, and O, respectively. See Table S1 for adsorption energies.

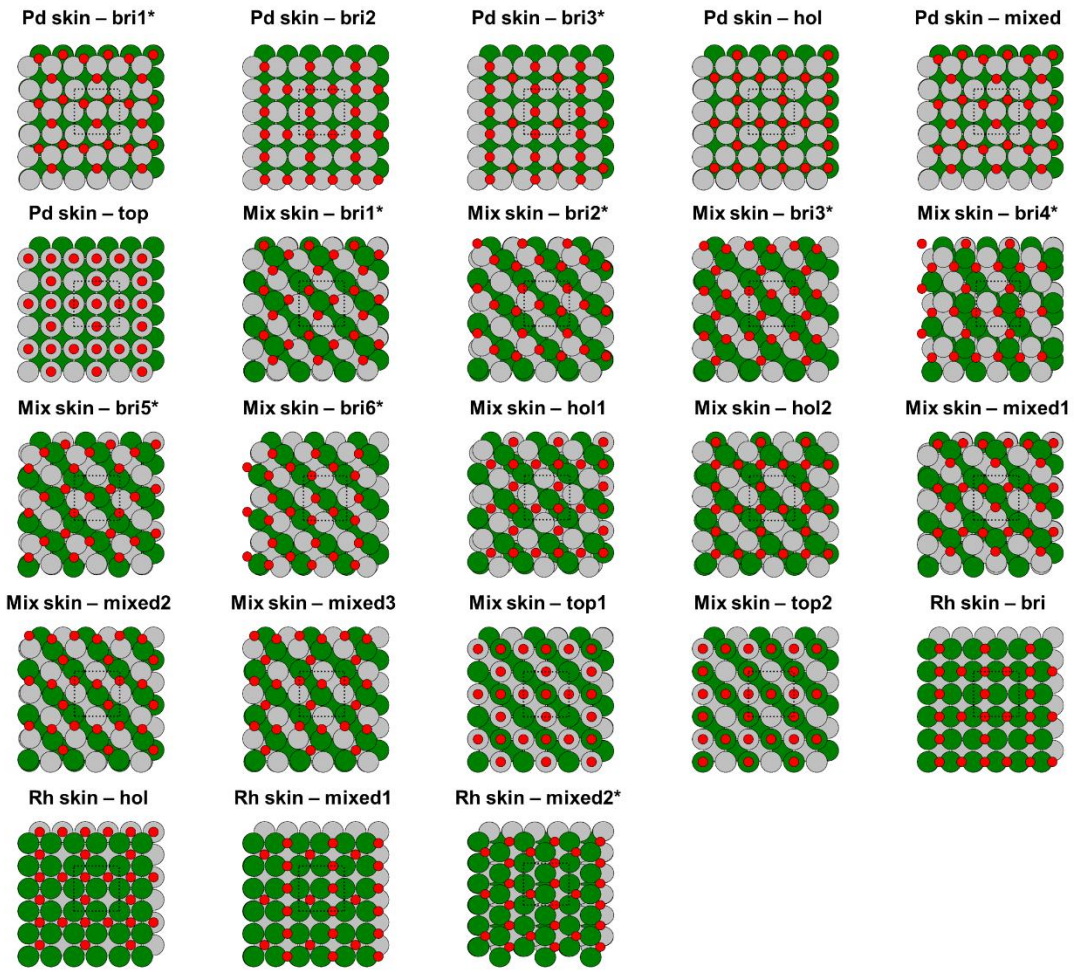

Figure S8. Top views of sites tested for 0.75 ML O* adsorption on $Rh_{50}Pd_{50}$(100). The silver, green, and red spheres represent Pd, Rh, and O, respectively. The sites marked with a * indicate site shifting upon optimization. See Table S2 for adsorption energies.

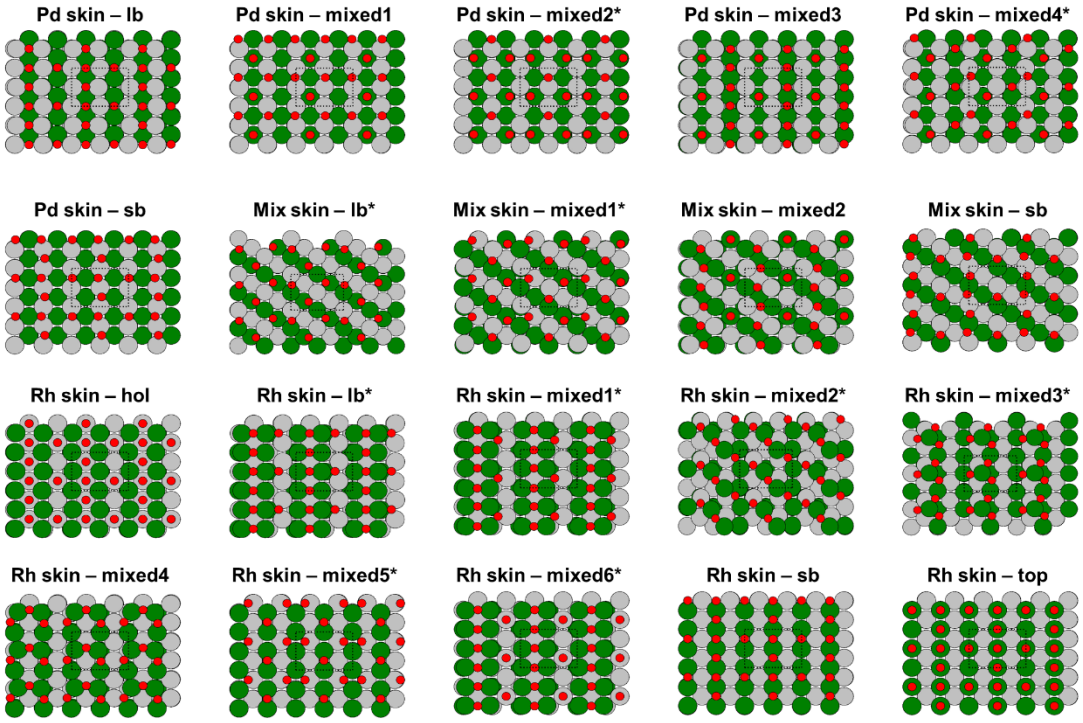

Figure S9. Top views of sites tested for 0.75 ML O* adsorption on $Rh_{50}Pd_{50}(110)$. The silver, green, and red spheres represent Pd, Rh, and O, respectively. The sites marked with a * indicate site shifting upon optimization. See Table S3 for adsorption energies.

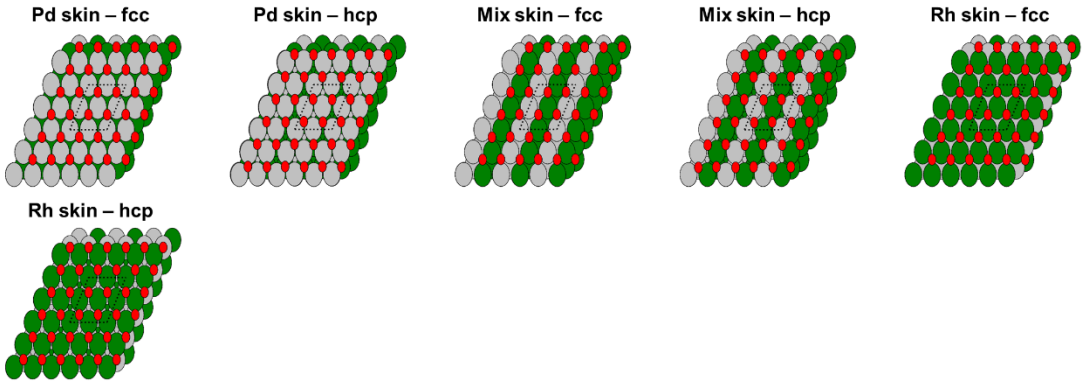

Figure S10. Top views of sites tested for 1.00 ML O* adsorption on $Rh_{50}Pd_{50}(111)$. The silver, green, and red spheres represent Pd, Rh, and O, respectively. See Table S1 for adsorption energies.

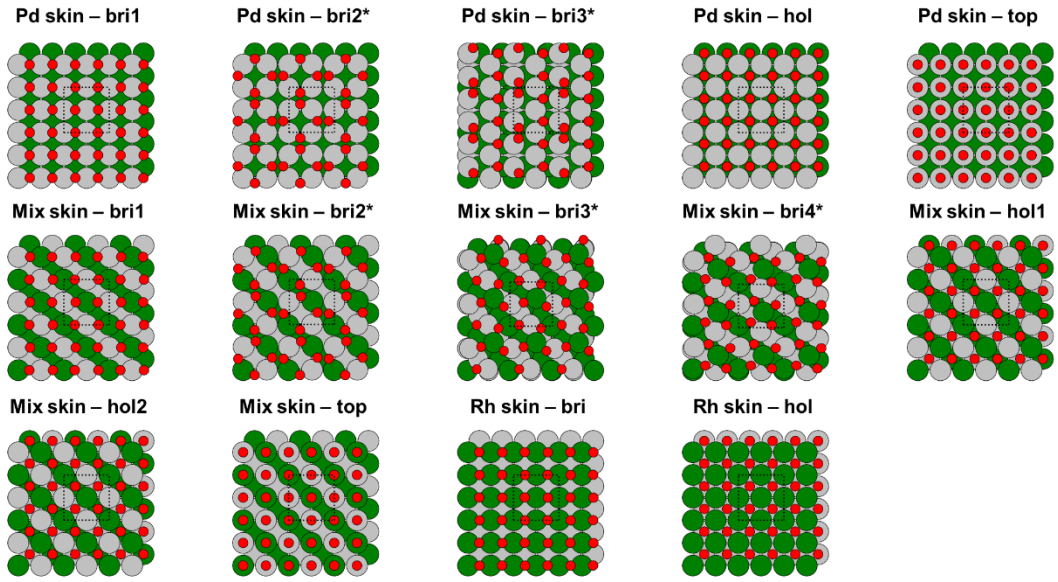

Figure S11. Top views of sites tested for 1.00 ML O* adsorption on $Rh_{50}Pd_{50}$(100). The silver, green, and red spheres represent Pd, Rh, and O, respectively. The sites marked with a * indicate site shifting upon optimization. See Table S2 for adsorption energies.

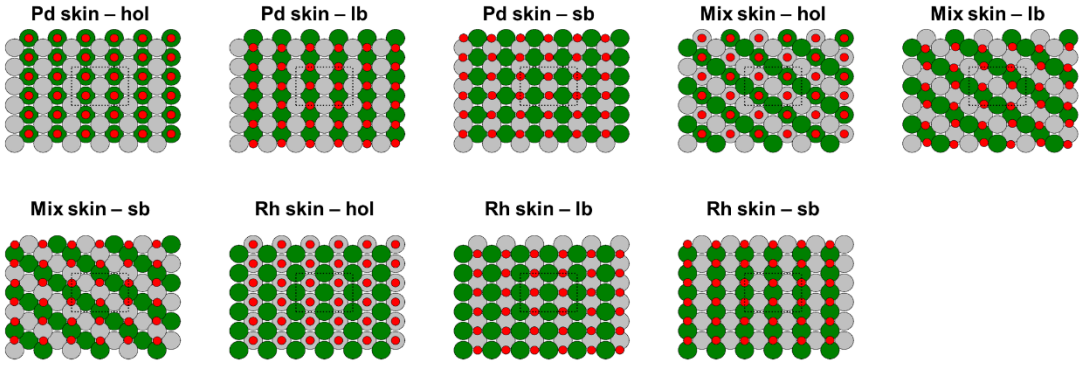

Figure S12. Top views of sites tested for 1.00 ML O* adsorption on $Rh_{50}Pd_{50}$(110). The silver, green, and red spheres represent Pd, Rh, and O, respectively. See Table S3 for adsorption energies.

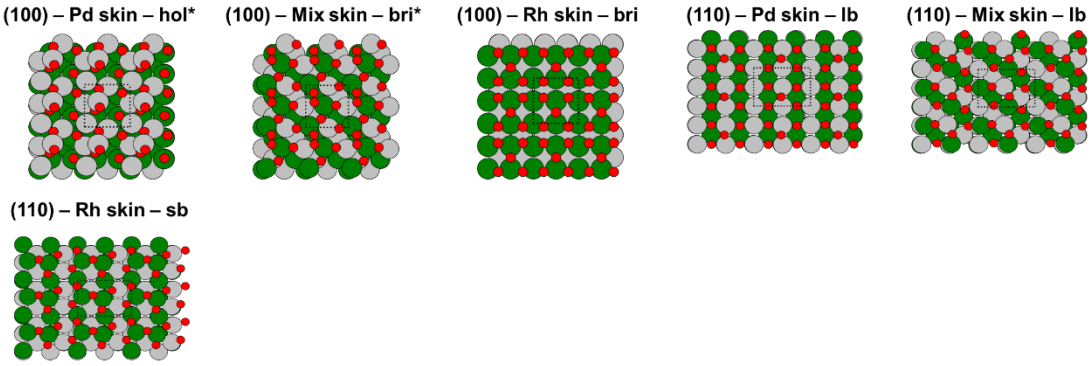

Figure S13. Top views of sites tested for 1.25 ML O* adsorption on $Rh_{50}Pd_{50}$(100) and (110). The sites marked with a * indicate site shifting upon optimization. The silver, green, and red spheres represent Pd, Rh, and O, respectively. See Tables S2-S3 for adsorption energies.

Table S1. Coverage-dependent adsorption and formation energies for O* on $Rh_{50}Pd_{50}$(111). Dominant adsorption configurations at each coverage are indicated in bold.

O* Coverage (ML)	Pd skin			Mix skin			Rh skin		
	Site Type	$E_{adsorption}$ (eV/O*)	$E_{formation}$ (eV)	Site Type	$E_{adsorption}$ (eV/O*)	$E_{formation}$ (eV)	Site Type	$E_{adsorption}$ (eV/O*)	$E_{formation}$ (eV)
0.00	-	-	**5.63**	-	-	**6.44**	-	-	**7.47**
0.25	bri*	-0.97	-	bri_{PdRh}*	-1.83	-	bri	-2.25	-
	fcc	**-0.97**	**4.66**	bri_{PdPd}*	-1.38	-	fcc	-2.20	-
	hcp	-0.79	-	**fcc_{RhRh}**	**-1.83**	**4.61**	**hcp**	**-2.25**	**5.23**
	top	0.43	-	fcc_{PdPd}	-1.38	-	top*	-2.28	-
	-	-	-	hcp_{PdPd}	-1.40	-	-	-	-
	-	-	-	hcp_{RhRh}	-1.73	-	-	-	-
	-	-	-	top_{Pd}*	-1.38	-	-	-	-
	-	-	-	top_{Rh}*	-1.73	-	-	-	-
0.50	**fcc**	**-0.70**	**4.23**	fcc1	-1.31	-	hcp	-1.91	-
	hcp	-0.45	-	fcc2	-1.31	-	**fcc**	**-2.01**	**3.46**
	mixed	-0.54	-	hcp1	-1.24	-	mixed	-1.80	-
	-	-	-	hcp2	-1.24	-	-	-	-
	-	-	-	hcp3	-1.36	-	-	-	-
	-	-	-	**mixed1**	**-1.39**	**3.65**	-	-	-
	-	-	-	mixed2	-1.03	-	-	-	-
0.75	**fcc**	**-0.38**	**4.51**	**fcc**	**-1.14**	**3.01**	hcp	-1.64	-
	hcp	-0.12	-	hcp	-1.01	-	**fcc**	**-1.76**	**2.20**
1.00	**fcc**	**0.00**	**5.65**	**fcc**	**-0.79**	**3.26**	hcp	-1.44	-
	hcp	0.31	-	hcp	-0.63	-	**fcc**	**-1.56**	**1.23**

Table S2. Coverage-dependent adsorption and formation energies for O* on $Rh_{50}Pd_{50}$(100). Dominant adsorption configurations at each coverage are indicated in bold.

O* Coverage (ML)	Pd skin			Mix skin			Rh skin		
	Site Type	$E_{adsorption}$ (eV/O*)	$E_{formation}$ (eV)	Site Type	$E_{adsorption}$ (eV/O*)	$E_{formation}$ (eV)	Site Type	$E_{adsorption}$ (eV/O*)	$E_{formation}$ (eV)
0.00	-	-	**7.19**	-	-	**8.52**	-	-	**9.58**
0.25	bri	-0.66	-	bri	-1.41	-	**bri**	**-2.03**	**7.55**
	hol	**-0.84**	**6.35**	hol_{Pd}	-1.64	-	hol	-1.90	-
	top	0.32	-	**hol_{Rh}**	**-1.71**	**6.80**	top	-0.88	-
	-	-	-	top_{Rh}	-1.06	-	-	-	-
	-	-	-	top_{Pd}	0.42	-	-	-	-
0.50	hol	-0.51	-	hol_{Rh}	-1.14	-	**bri**	**-1.93**	**5.72**
	bri	-0.49	-	bri	-1.31	-	hol	-1.81	-
	mixed	**-0.51**	**6.16**	**mixed1***	**-1.52**	**5.47**	mixed*	-1.93	-
	-	-	-	mixed2*	-1.52	-	-	-	-
0.75	hol	-0.15	-	hol2	-0.80	-	bri	-1.62	-
	bri1*	-0.16	-	bri1*	-0.91	-	hol	-1.36	-
	bri2	-0.22	-	bri2*	-0.96	-	**mixed1**	**-1.62**	**4.72**
	bri3*	**-0.28**	**6.35**	**bri3***	**-1.05**	**5.38**	mixed2*	-1.84	-
	top	0.69	-	bri4*	-1.25	-	-	-	-
	mixed	-0.16	-	bri5*	-0.93	-	-	-	-
	-	-	-	bri6*	-1.05	-	-	-	-
	-	-	-	hol1	-0.87	-	-	-	-
	-	-	-	top1	0.23	-	-	-	-
	-	-	-	top2	-0.29	-	-	-	-
	-	-	-	mixed1	-0.94	-	-	-	-
	-	-	-	mixed2	-1.03	-	-	-	-
	-	-	-	mixed3	-1.05	-	-	-	-
1.00	hol	-0.23	-	hol2	-0.70	-	**bri**	**-1.43**	**3.87**
	bri1	**-0.02**	**7.09**	**bri1**	**-0.75**	**5.51**	hol	-1.06	-
	bri2*	-0.22	-	bri2*	-0.56	-	-	-	-
	bri3*	-0.22	-	bri3*	-0.83	-	-	-	-
	top	0.85	-	bri4*	-0.91	-	-	-	-
	-	**-**	**-**	hol1	-0.70	-	**-**	**-**	**-**
	-	**-**	**-**	top	0.09	-	**-**	**-**	**-**
1.25	hol*	-0.12	-	bri*	-0.64	-	**bri**	**-1.01**	**5.54**

Table S3. Coverage-dependent adsorption and formation energies for O* on $Rh_{50}Pd_{50}$(110). Dominant adsorption configurations at each coverage are indicated in bold.

O* Coverage (ML)	Pd skin			Mix skin			Rh skin		
	Site Type	$E_{adsorption}$ (eV/O*)	$E_{formation}$ (eV)	Site Type	$E_{adsorption}$ (eV/O*)	$E_{formation}$ (eV)	Site Type	$E_{adsorption}$ (eV/O*)	$E_{formation}$ (eV)
0.00	-	-	**11.07**	-	-	**11.58**	-	-	**12.43**
0.25	hol	-0.89	-	hol_{Rh}	-0.94	-	hol	-0.57	-
	lb	**-1.26**	**9.81**	hol_{Pd}	-0.44	-	lb	-1.33	-
	sb	-0.69	-	lb	-0.80	-	**sb**	**-2.05**	**10.37**
	top	0.17	-	**sb**	**-1.46**	**10.12**	top	-0.93	-
	-	-	-	top_{Pd}	0.36	-	-	-	-
	-	-	-	top_{Rh}	-1.05	-	-	-	-
0.50	**lb**	**-1.08**	**8.92**	sb	-1.49	-	**sb**	**-2.08**	**8.26**
	sb	-0.64	-	lb*	-1.47	-	lb	-1.36	-
	hol	-0.80	-	hol_{Rh}	-0.87	-	hol	-0.43	-
	mixed1	-0.91	-	mixed1*	-1.22	-	mixed1*	-1.37	-
	mixed2	-1.07	-	**mixed2***	**-1.51**	**8.56**	mixed2*	-2.08	-
0.75	lb	-0.86	-	sb	-1.09	-	**sb**	**-1.67**	**7.42**
	sb	-0.39	-	**lb***	**-1.53**	**7.00**	hol	-0.44	-
	mixed1	-0.56	-	mixed1*	-1.14	-	lb*	-1.27	-
	mixed2*	-0.81	-	mixed2	-0.77	-	top	-0.85	-
	mixed3	**-0.90**	**8.38**	-	-	-	mixed1*	-1.45	-
	mixed4*	-0.83	-	-	-	-	mixed2*	-1.58	-
	-	-	-	-	-	-	mixed3*	-1.46	-
	-	-	-	-	-	-	mixed4	-1.64	-
	-	-	-	-	-	-	mixed5*	-1.39	-
	-	-	-	-	-	-	mixed6*	-0.98	-
1.00	**lb**	**-0.88**	**7.56**	sb	-0.90	-	**sb**	**-1.46**	**6.58**
	sb	-0.26	-	**lb**	**-0.90**	**7.97**	lb	-0.93	-
	hol	-0.69	-	hol	-0.44	-	hol	-0.32	-
1.25	**lb**	**-0.87**	**7.58**	**lb**	**-1.10**	**7.17**	**sb**	**-1.70**	**5.64**

Table S4. Linear regression models and errors for predicting average O* adsorption energy on $Rh_{50}P_{50}$(111), (100), and (110) model surfaces. The system with the largest RMSE is indicated in bold.

System	Slope (eV/O*/ML)	Intercept (eV/O*)	RMSE (eV/O*)	MAE (eV/O*)
(111) – Pd skin	1.3014	-1.3248	0.03	0.03
(111) – Mix skin	1.3442	-2.1298	0.04	0.03
(111) – Rh skin	0.9244	-2.4708	0.01	0.01
(100) – Pd skin	1.0728	-1.0845	0.02	0.02
(100) – Mix skin	1.3452	-2.0990	0.06	0.05
(100) – Rh skin	1.0153	-2.3645	0.07	0.07
(110) – Pd skin	0.3878	-1.2878	0.06	0.05
(110) – Mix skin	**0.5331**	**-1.7016**	**0.17**	**0.15**
(110) – Rh skin	0.5339	-2.1930	0.15	0.13

Table S5. Parabolic regression models and errors for predicting surface formation energy of O* covered $Rh_{50}P_{50}$(111), (100), and (110) model surfaces. Parabola fit to: $E_{formation} = A\theta^2 + B\theta + C$. The system with the largest RMSE is indicated in bold.

System	A (eV/ML^2)	B (eV/ML)	C (eV)	RMSE (eV)	MAE (eV)
(111) – Pd skin	5.6333	-5.6841	5.6647	0.05	0.04
(111) – Mix skin	5.1212	-8.2987	6.4213	0.06	0.05
(111) – Rh skin	3.4873	-9.6920	7.4571	0.03	0.03
(100) – Pd skin	4.0292	-4.1060	7.1688	0.03	0.02
(100) – Mix skin	5.6446	-8.6171	8.5273	0.10	0.09
(100) – Rh skin	6.4137	-11.7010	9.8025	0.34	0.29
(110) – Pd skin	1.9127	-5.2210	11.0547	0.11	0.08
(110) – Mix skin	**3.8478**	**-8.2437**	**11.6811**	**0.42**	**0.33**
(110) – Rh skin	3.0517	-9.0887	12.3816	0.19	0.16

Table S6. Linear regression models and errors for predicting vibrational energy of O* covered $Rh_{50}P_{50}$(111), (100), and (110) model surfaces. The system with the largest RMSE is indicated in bold.

System	Slope (eV/ML)	Intercept (eV)	RMSE (eV)	MAE (eV)
(111) – Pd skin	0.0855	-1.1867	0.02	0.02
(111) – Mix skin	0.3397	-1.3501	0.06	0.05
(111) – Rh skin	0.3757	-1.3496	0.03	0.03
(100) – Pd skin	0.0131	-1.3192	0.02	0.02
(100) – Mix skin	0.0579	-1.3724	0.03	0.03
(100) – Rh skin	-0.1083	-1.3234	0.06	0.05
(110) – Pd skin	-0.3661	-1.8317	0.08	0.06
(110) – Mix skin	**-0.3838**	**-1.7797**	**0.11**	**0.10**
(110) – Rh skin	-0.4894	-1.7809	0.05	0.05

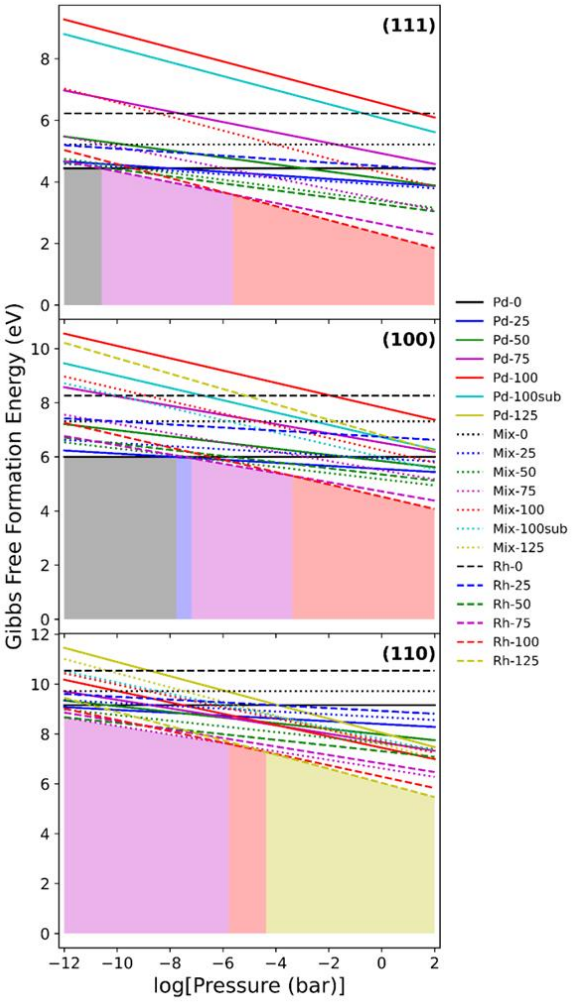

Figure S14. 2D phase diagrams of O* covered $Rh_{50}Pd_{50}$(111), $Rh_{50}Pd_{50}$(100), and $Rh_{50}Pd_{50}$(110) under reaction temperature of 573.15 K while varying O_2 partial pressure (10^{-12}-10^{2} bar). Bulk Rh and Pd as well as ½ gas phase O_2 are the $\Delta G = 0$ eV references. The solid, dotted, and dashed line denotes Rh-Pd surface structures with Pd, Mix, and Rh skin, respectively. Designated color codes represent different O* surface coverages (black: 0.00 ML; blue: 0.25 ML; green: 0.50 ML; purple: 0.75 ML; red: 1.00 ML; cyan: 1.00 ML subsurface diffusion; yellow: 1.25 ML). Shade areas indicate corresponding dominant O* covered/clean Rh-Pd surface structures within specific pressure ranges. Possible metastable states for each facet were identified by determining the surface structures within +-0.5 eV of the dominant phases. For (111), the metastable states are: (low pressure) Mix-25>Rh-50>Rh-75>Pd-25>Mix-50>Rh-100; (high pressure) Rh-50>Rh-100>Mix-50>Mix-25>Pd-0>Pd-25 and Rh-75>Rh-50>Mix-50. For (100), the metastable states are: (low pressure) Mix-50>Rh-75>Rh-50>Mix-25> Rh-100; (high pressure) Rh-100>Mix-50>Pd-25>Rh-50>Pd-0. For (110), the metastable states are: (low pressure) Rh-50>Rh-75>Rh-100>Mix-50>Pd-25>Pd-0; (high pressure) Rh-100>Mix-75>Rh-75.

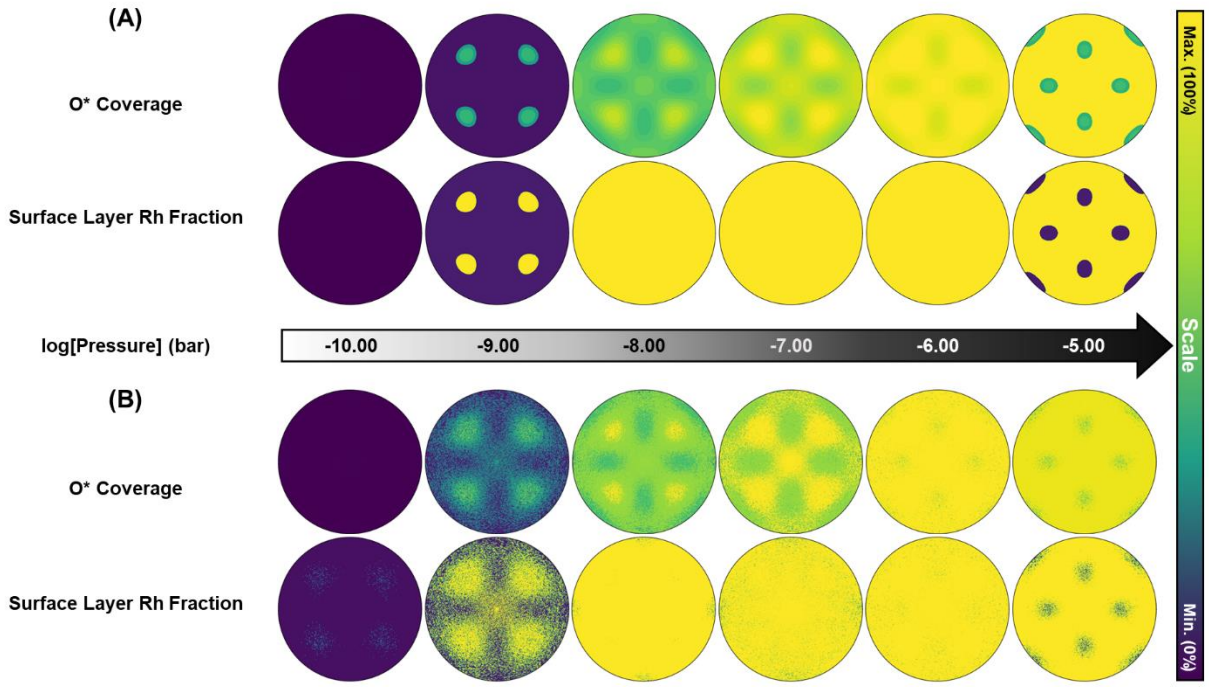

Figure S15. Analysis of the impact of DFT-level errors (i.e. from regression models for adsorption, formation, and Gibbs free energy) on equilibrium O* coverage and surface layer Rh fraction in $Rh_{50}Pd_{50}$ multi-faceted catalytic nanoparticles The temperature was set to 573.15 K and O_2 partial pressures ranged from 10^{-10}-10^{-5} bar. The scale bar represents intensity from a percentage of 0 (purple) to 100 (yellow). (A) No error introduced; (B) Error introduced from the largest RMSEs calculated for adsorption (0.17 eV/O*), formation (0.42 eV), and vibrational Gibbs free energy (0.11 eV). Data are summarized in Tables S4-S6.

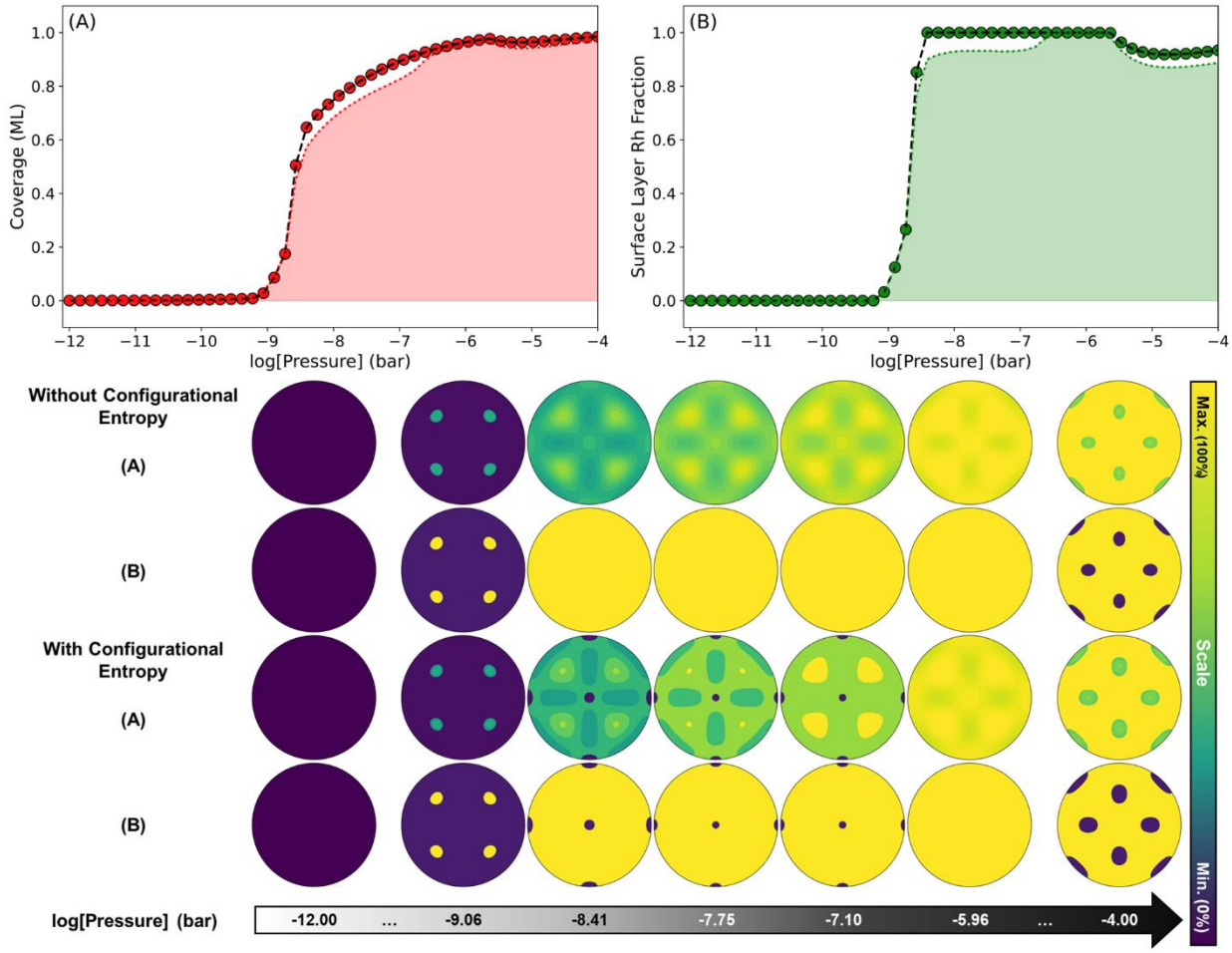

Figure S16. Effect of configurational entropy $\Delta S_{conf} = k_B \, ln\left(\frac{1-\theta_{O*}}{\theta_{O*}}\right)$ on the equilibrium O* coverage and surface layer Rh fraction for $Rh_{50}Pd_{50}$ nanoparticle models. The temperature was set to 573.15 K and O_2 partial pressure ranged from 10^{-12}-10^{-4} bar. Dashed lines with markers represent nanoparticle model results without configurational entropy. Dotted lines with shaded areas indicate nanoparticle model results with configurational entropy under same conditions. (A) Surface O* coverage; (B) Surface layer Rh fraction.

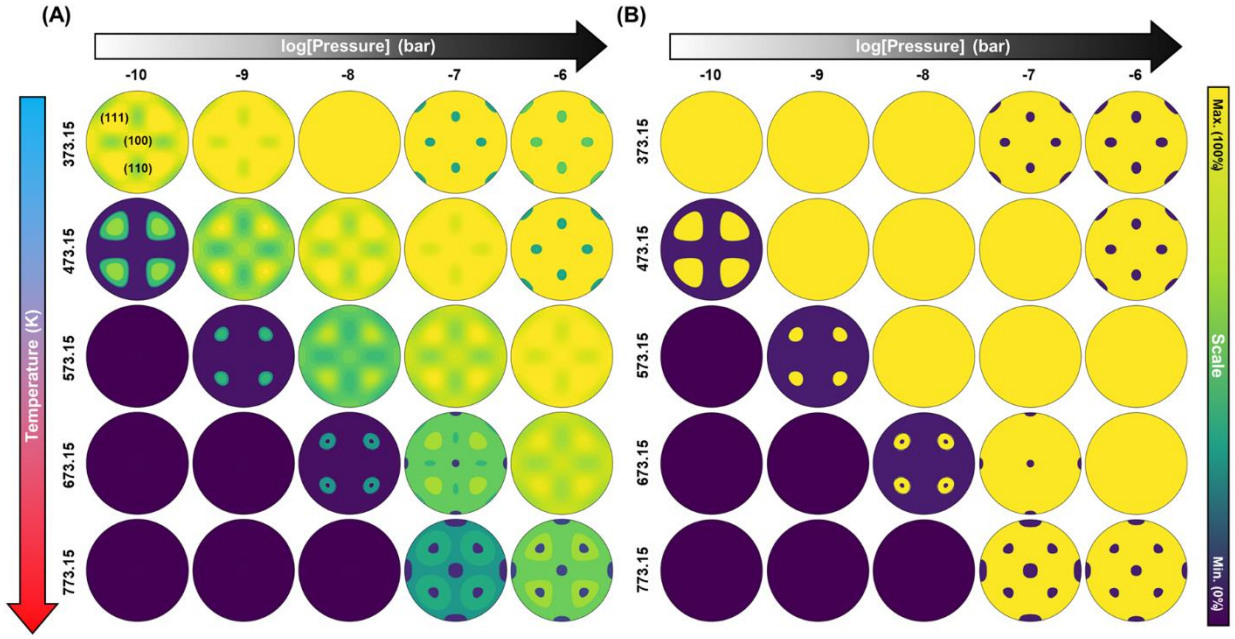

Figure S17. Full temperature and pressure dependence on equilibrium O* coverage and surface layer Rh fraction for $Rh_{50}Pd_{50}$ nanoparticle models. The temperature was set to 373.15-773.15 K and O_2 partial pressure ranged from 10^{-10}-10^{-6} bar simultaneously. (A) Surface O* coverage; (B) Surface layer Rh fraction.

Extent of Reaction Calculations for Effective O_2 Partial Pressures

To compare our $Rh_{50}Pd_{50}$ nanoparticle reconstruction models to the relevant experiments, we must determine the equivalent O_2 partial pressures required to reproduce the experimental oxidizing and reducing gas phase environments. Here, we take the oxidizing condition, i.e. 1.33×10^{-4} bar NO(g), at 473.15 K as a case study to demonstrate our extent of reaction calculation approach. In this scenario, NO(g) dissociates into N_2(g) and O* onto the $Rh_{50}Pd_{50}$ nanoparticle. As O* can also be produced from the dissociative adsorption of O_2(g), the effective O_2(g) pressure required to obtain an equivalent amount of O* as 1.33×10^{-4} bar of NO(g) under equilibrium conditions can be determined by solving for the extent of reaction for $2NO(g) \rightarrow N_2(g) + O_2(g)$. For this gas phase reaction, the extent of reaction (ε) can be related to the equilibrium constant by:

$$K_{eq} = \frac{y_{N_2} y_{O_2}}{y_{NO}^2} = \frac{\left(\frac{\varepsilon}{P_{NO,ini}}\right)\left(\frac{\varepsilon}{P_{NO,ini}}\right)}{\left(\frac{P_{NO,ini} - 2\varepsilon}{P_{NO,ini}}\right)^2} = \frac{\varepsilon^2}{\left(P_{NO,in} - 2\varepsilon\right)^2} \tag{S1}$$

The equilibrium constant is related to the Gibbs free energy of reaction by:

$$K_e = \exp\left(-\frac{\Delta G_{rxn}}{k_b T}\right) \tag{S2}$$

Thus, we must calculate the Gibbs free energies for gas phase NO, N_2, and O_2, which can be obtained from:

$$\begin{aligned} \Delta G_{rxn} &= \Delta G_{O_2} + \Delta G_{N_2} - 2G_{NO} \\ &= E_{rxn}^{DFT} + \Delta G_{O_2}^{correction}(T, P_{O_2}) + \Delta G_{N_2}^{correction}\left(T, P_{N_2}\right) \\ &\quad - 2\Delta G_{NO}^{correction}(T, P_{NO}) \end{aligned} \tag{S3}$$

where E_{rxn}^{DFT} is the reaction energy calculated at the DFT-level, while $\Delta G_{O_2}^{correction}(T, P_{O_2})$, $\Delta G_{N_2}^{correction}(T, P_{N_2})$, and $\Delta G_{NO}^{correction}(T, P_{NO})$ and the Gibbs free energy corrections from vibrational, rotational, and translational motion for gas phase O_2, N_2, and NO, respectively.

By examining Equations S1-S3, it is clear that this problem must be solved self-consistently by guessing extents of reaction until the left- and right-hand sides of Equation S1 are equal. This was accomplished using Excel's Solver function. For $2NO(g) \rightarrow N_2(g) + O_2(g)$ at 473.15 K, the resulting extent of reaction was 6.67×10^{-5} bar, which is consistent with the highly exergonic Gibbs free energy of reaction. Thus, the effective equilibrium O_2(g) partial pressure is 6.67×10^{-5} bar for an applied 1.33×10^{-4} bar of NO(g) at 473.15 K. Results for all oxidizing and reducing conditions are shown in Table S7.

Table S7. Summary of extent of reaction calculations used to determine the effective O_2 partial pressures under applied oxidizing ($2NO(g) \rightarrow N_2(g) + O_2(g)$) and reducing ($H_2(g) + \frac{1}{2}O_2(g) \rightarrow H_2O(g)$) conditions. Temperature and initial pressures (either NO or H_2) were taken from experiments by Tao et al.[1]

Conditions	Temperature (K)	P_{ini} (bar)	ΔG_{rxn} (eV)	ε (bar)	$P_{O_2}^{effective}$ (bar)
Oxidizing (applied NO)	473.15	1.33×10^{-4}	-1.151	6.67×10^{-5}	6.67×10^{-5}
Reducing (applied H_2)	473.15	1.33×10^{-4}	-1.007	1.33×10^{-4}	2.54×10^{-10}
Oxidizing (applied NO)	573.15	1.33×10^{-4}	-1.131	6.67×10^{-5}	6.67×10^{-5}
Reducing (applied H_2)	573.15	1.33×10^{-4}	-0.954	1.33×10^{-4}	3.85×10^{-9}

References

1. F. Tao, M. E. Grass, Y. Zhang, D. R. Butcher, J. R. Renzas, Z. Liu, J. Y. Chung, B. S. Mun, M. Salmeron and G. A. Somorjai, *Science*, 2008, **322**, 932-934.